Interaction between alkali metals and diamond: etching and charge states of NV centers

Hiroki Takehana[1], Ichiro Yamane[1], Takashi Yanase [1,2], Taro Nagahama [1,2] and Toshihiro Shimada [1,2]

[1] *Graduate School of Chemical Sciences and Engineering, Hokkaido University, Kita13 Nishi8, Kita-ku, Sapporo, 060-8628, Japan*

[2] *Graduate School of Engineering, Hokkaido University, Kita13 Nishi8, Kita-ku, Sapporo, 060-8628, Japan*

Abstract

Single crystal diamond particles were heated with liquid phase alkali metals (Li, Na, K) in an argon atmosphere. It was found that Li reacts with the diamond above 600 ºC, Na makes the surface rougher on a nm scale at 800 ºC, and K did not change the surface morphology. The etching speed by the reaction with Li is the fastest on the (001) surface. Photoluminescence of the NV^- (negatively charged nitrogen-vacancy) center decreased only after the annealing with K. DFT calculations explained the strong chemical interaction between Li and the diamond (001) surfaces, and upward band bending at the interfaces with Na and K. The behavior of the NV^- center photoluminescence is consistent with the extent of band bending.

Keywords: diamond, alkali metals, NV center, etching, band bending

e-mail: shimadat@eng.hokudai.ac.jp

1. Introduction

Reactions and electronic interactions between diamond surfaces and metals are important in the application of the diamond as mechanical tools, and in thermal, electronic and quantum devices[1–4]. Stable bonding of diamond particles with metals via interface carbides are critical to fabricating machining tools[5,6]. The very high thermal conductivity of the diamond [2,6,7], which reaches maximum of 410W/cm K at 104 K when isotopically enriched, but theoretically higher is expected [2], has attracted research efforts on its composites with high thermal-conductivity metals and oxides [8–11]. Ohmic contacts, Schottky barrier formation and surface charge accumulations play essential roles in the electronics application of the diamond in power devices[3,12–17] and radiation sensors[18–20]. Quantum devices using nitrogen-vacancy (NV) centers are intensively studied as a candidate for a quantum bit and in extremely sensitive magnetic, thermal, and chemical sensors[21–25]. Controlling the charge states of the NV-centers by surface modification is important, and various methods have been reported[26–35]. The catalytic functions and chemical solubility of metals at the diamond interfaces can also be used for the precise machining of diamonds[36-40]. Since the diamond is chemically strong in reducing environments, there are many attempts to use it in rechargeable batteries using alkali metals, especially lithium[41,42]. It is important to examine the reactivity of diamond with alkali metals at elevated temperatures.

However, the interaction of diamond with alkali metals has not been studied in detail to the best of the authors' knowledge. In this study, we experimentally evaluated the interaction between diamond and molten alkali metals (Li, Na, K) at elevated temperatures (500 - 800 ^{o}C) by heating alkali metals and diamond crystals in argon-filled niobium tubes. The surface morphology after the interaction was studied in detail. The photoluminescence of the NV centers was used as a probe of their charge states, which indicates the electronic interactions during the alkali metal annealing. Based on density functional theory (DFT) calculations, we confirmed that the observed interactions, including the strong reactivity of Li and electron extracting tendency from a NV^- center, can be reasonably explained.

2.Experiment

The reaction tube used in the experiments is shown in Fig. 1(a). The sample was prepared in a glove box under an Ar atmosphere (<50ppm H_2O). Li (Kanto Chemical, 99%), Na (Sigma-Aldrich 99.8%), and K (Sigma-Aldrich 98%) were cut to the appropriate size (> 0.3 cm^3) and washed in hexane in the glove box. The diamond was HPHT (high pressure high temperature) -synthesized particles (diameter ~300 μm) which contained nitrogen as an impurity, which was purchased from Global Diamond Co., Ltd., Tokyo, Japan. The diamond particles were single crystals and their low-index faces can be recognized using a low magnification optical microscope (Fig.1(b)). The density of the nitrogen impurities of the diamond particles was evaluated by microfocus SIMS (Isotope Microscope, Hokkaido University) using an HPHT single crystal (SumiCrystal, Sumitomo Electric Industries) as a reference. It was found to be in the range of 30 - 60 ppm.

A Nb tube (Nilaco, 99.9%) with an inner diameter of 5mm was welded at one side in advance and washed with acetone. Since we found that the photoluminescence of the NV centers was dependent on the particles and the positions in each particle, we chose one piece of the diamond particle with well-developed crystal surfaces for each experiment. It was thoroughly characterized as described below and then put in the Nb tube along with an excess alkali metal chunk. The end of the Nb tube was then pressed flat and welded for vacuum tight sealing. All the above processes were done in the Ar glove box. In order to prevent oxidation of the Nb capsule, it was put in a quartz ampoule, and sealed in a rotary-pump-vacuum by a hydrogen-oxygen flame. We prepared 4 types of samples, *i.e.*, diamond particles processed with Li, Na, K, and without any alkali metal (vacuum-sealed in the quartz ampoule).

The samples in the quartz ampoule were heated at 800 ºC for 24 hours. For Li, which reacted with the diamond, lower temperatures and shorter periods were employed as described in the next section. After the heating, the quartz ampoules and Nb capsules were opened in the glove box, and the diamond particles were washed with ethanol and then water. A laser microscope (Keyence VK-8170) and a Raman microscope (Renishaw inVia Reflex AP, 532 nm excitation) were used for the characterization of the surface morphology and photoluminescence of the NV^0 and NV^- centers. It is noted that the boiling points of Li, Na, K are 1330 ºC, 882.8 ºC and 758.8 ºC, respectively. Considering the amount of alkali metals (~30% of the Nb capsule), the vaporization molar ratio at 800 ºC (less than

1/1000 even for K) and the experimental geometry, the diamond particles were immersed in the alkali metals in the liquid phase.

We measured the X-ray Photoelectron Spectra (XPS) of the diamond grains with and without the Na and K annealing (800 ºC, 24h) treatments. The samples were attached to an indium foil by mechanically pressing against the foil by holding their sides. A JEOL JPS-9200 spectrometer with Mg Kα X-rays and 0.2 mm spot size was used for the measurement.

The interface structures and electronic structures were calculated using the DFT package VASP[43]. PBE functional[44] and ultrasoft pseudopotential [45,46] were used with the augmented plane wave method. The initial structure for the optimization was created considering the bulk lattice constants of the Li, Na, and K. 3×3×4 unit cells of the diamond with 4 layers of alkali metal atoms on both sides were employed. The lattices of the alkali metals of the initial structures were from a 10.4% compression to 2.4% expansion in comparison to the bulk density. We tried several starting structures of the alkali metals (lattice orientation and symmetry), and the final structure was almost the same after the energy optimization. 10 Å of vacuum was placed between the slab (alkali metal - diamond - alkali metal). The structure was optimized to make the force below 50 meV/Å. 4×4×1 k-point grids were used for the electronic calculations. The local density of states (LDOS) of each atomic layer was extracted from the VASP results using the python libraries of the "Materials Project"[47].

3. Results

3.1 Chemical reactivity of diamond and alkali metals

Figure 2 shows the laser microscopy images of the same diamond microcrystals before (a, c, e) and after (b, d, f) annealing with the alkali metals. The temperature and time were 650 ºC and 20min for Li (Figs.2b), and 800 ºC and 24 h for Na (Figs. 2 d) and K (Figs. 2 f), respectively. Substantial etching was observed for the Li and a hexagonal-triangular etch pattern was evident. When the diamond and Li were heated at higher temperatures or a longer time, the diamond crystal disappeared. For Na, the images show a slight difference; Fig. 2d shows brighter

lines than Fig. 2c. This difference is evidenced by the 3D roughness evaluation using the laser microscope by an automatic focal position distribution measurement (root-mean-square roughness 5.0 nm vs 8.5 nm for Figs.2 c and d, respectively). K did not show this difference in the image and showed no change in the surface roughness. This result indicated that the reactivity of Li, Na, and K with the diamond decreases in this order. The etch rate of diamond with Li, Na, and K is >> 10^5 nm/day, a few nm/day (difference in the roughness of Figs.2c and d), and << 1nm/day at 800 ºC, resepectively.

We next examined the etching behavior of Li in detail. Figure 2b shows the characteristic structure with 120º rotated edges. It seems that the (111) surface remained. We obtained 3D surface images using the laser microscope and created virtual cross sections. Their typical images are shown in Fig. 3. The right panel of Fig. 3 shows the characteristic angles of 35º and 70º, which were frequently observed. These angles correspond to those between {111} and {110} (35.26º), and between {111} and $\{11\bar{1}\}$ (70.52º), respectively. Other angles, such as 90º (the angle between {100} and {010}), 54.73º ({111} and {100}) or 45º ({110} and {100}) were not observed. This result indicated that the etching speed of the {100} surface by Li is much higher than those of the {111} or {110} surfaces.

For application in lithium ion batteries, it is important to determine the temperature at which the etching starts. We examined the temperature using the following procedure: The Nb tube containing the Li-diamond mixture was first heated to 350ºC. The temperature was then ramped to the target temperature (T) in 3 hours at a constant increasing rate, and it was maintained at T for 20 min, then cooled by turning off the furnace. The results are shown in Fig. 4. The T=550 ºC (not shown) did not make a noticeable change in the morphology. At T =600ºC (Figs.4 ab), the etching started where the surface was not flat, but the flat region did not significantly change. At T =625ºC (Figs.4cd), the etching seemed to occur even on the flat surface. Since the etching involves nucleation of the etching sites, it is difficult to quantitatively identify the threshold temperature and the involved parameters from the experiment. Practically, we concluded that 600ºC is the temperature when the etching start in the time scale of tens of minutes.

The etching of a diamond surface has been studied regarding the catalytic oxidation with a Ni film[36], at the

melt interfaces with KNO_3[40] or in an aqueous solution (KCl + KOH)[48] but no reports are found about the reducing conditions. We noted that the etching reaction by Li occurs at a much lower temperature compared to that by oxidation or by dissolution in lanthanoid metals[49].

3.2 Change in NV center charges

Figure 5 shows the photoluminescence of the NV centers measured with a 532nm excitation. The graphs illustrate the typical data of (a) vacuum annealing at 800 ºC for 24 hours, (b)Li treatment at 500 ºC for 24 hours (no significant etching), (c) Na and (d) K treatments at 800 ºC for 24 hours. The insets depict the NV^- peaks after subtracting the broad background due to phonon-involved fluorescence and normalizing by the peak area around 573 nm (diamond Raman and NV^0, see below). We noticed that the fluorescence intensity was dependent on the diamond microcrystals and the positions of each microcrystal, thus we measured the same positions under ×50 objective lens before and after the annealing treatment. Six ~ 12 samplings were employed and the results were statistically analyzed.

We noted that almost no changes were observed in the cases of vacuum annealing and the Li and Na treatments (Figs.5a-c). The change in the normalized intensity of NV^- (as shown in the insets) was negligible, which was less than ±20% for all of the measured samples and positions. After the K treatment, however, a broad feature around 620 nm appeared and the NV^- zero-phonon fluorescence (637nm, denoted as NV^- in Fig. 5d) decreased (by -52% in statistical average). The Raman signal of diamond (1333cm^{-1}, 573 nm) coincides with the zero-phonon fluorescence of NV^0 (575 nm). A broad feature around 620nm (centered at 650 nm) has been assigned as phonon-involved fluorescence from NV^0 (denoted as $NV^{0'}$ in Fig.5d) in the literature[29,50]. The increase in $NV^{0'}$ associated with the decrease in NV^- is reasonably explained by the change in the charge state. It is contradictory to the fact that K has the lowest electronegativity among the three alkali elements and is a strongly electron-donating agent in chemistry. This point will be clarified in the next section with the aid of DFT calculations.

We admit that the difference shown in Fig.5d is not high and there might be other explanations. Especially, the position of the feature at 620 nm coincides with the second order Raman of diamond (2664 cm^{-1})[51]. However,

the shape and relative intensity of the peak are not identical to that of the reported second order Raman. It is difficult to regard this feature as other carbon-related Raman or fluorescence because the G-band (1500-1600cm^{-1}, corresponding to 578-581nm) is not observed. It is desirable if an optically-detected magnetic resonance measurement can be performed before and after the alkali-metal treatments, but we found that the sample alignment to both the microwave and the laser was very severe for the 300μm grain-shaped samples. Therefore, we present the experimental results with one plausible explanation (change in NV^0/NV^- ratio) as stated in this section.

3.3 Surface analysis by XPS

Figure 6 shows the XP spectra of C1s and O1s as non-treated and after annealing with Na and K. We confirmed that the macroscopic surface charging effect during the XPS was not severe by using a neutralization gun. It is noted that the non-treated and K-annealed samples show a similar peak position of C1s (binding energy (E_B) ~ 288 eV), which is characteristic of a single crystal diamond showing a microscopic charging effect [52]. The Na-treated sample shows the C1s peak with lower E_B (285~287 eV) with broadening. It indicated that the carbon at the surface partially changed its chemical or electrical nature, which resembles amorphization[53]. O1s shows a similar lowering of the peak E_B only for the Na-annealed samples. The O/C peak area ratios were 0.59, 0.44, and 0.37 for the non-treated, Na-annealed, and K-annealed samples, respectively.

4. Discussion

The reaction of alkali metals with a diamond surface has not been systematically studied to the best of the authors' knowledge. Only Li_2C_2 is known as an alkali metal carbide[54]. We found the comparison of the formation energy for Li_2C_2 and hypothetical Na_2C_2 and K_2C_2 by DFT calculations from the alkali metals and graphite, which gives the values of 0.015eV, 0.241 eV, and 0.250 eV, respectively[47]. The formation energy of diamond from graphite is 0.136 eV[55], and by subtraction of this value, the reaction energy of Li, Na and K with the diamond yields -0.121 eV, +0.105eV and +0.114 eV, respectively. It reasonably accounts for the reactivity of Li, Na, and K with the diamond surface.

We performed DFT calculations of the alkali metal / diamond (100) interface to elucidate the nature of the strange behavior of the charge states of the NV center. We have calculated 4 atom layers of alkali metals (Li, Na, K) on a diamond 4 atomic layer-thick (100) slab, which is half of the symmetric unit of the calculation. The structure was optimized starting from various initial arrangements. We then calculated the electronic structure. We found that the optimized structure converged to a structure specific to each alkali metal. They are shown in Fig. 7. It is noted that Li atoms at the interface are located much closer to the diamond surface than the Na and K, and two layers (Li3 and Li4) are at the same height. This feature specific to Li is probably related to the strong chemical interaction between the Li and carbon atoms.

The local density of states (LDOS) of the atomic layers are presented in Fig. 8 to examine the electronic structure at the interfaces. The Fermi levels are located at $E = 0$. The numbers of atomic layers are indicated in Fig. 7. The LDOSs of the alkali metal layers far from the interface (Li1, Na1, Na2, K1 and K2) are almost identical to the second layer from the interface (Li2, Na3 and K3, respectively); they are not shown in Fig. 8. This result indicated that the thickness of the alkali metal layers was sufficient to take the bulk of the alkali metals into account.

It is easily noticed that the Li interface gives distinctly different LDOS features from those of the interfaces with Na and K. This indicated the strong chemical interaction between Li and the diamond surface. The diamond interfaces with Na and K have similar features. C1 shows hybridized states near the Fermi level (E= -0.5~+0.5 eV) and these gap states decay as the distance from the interface increases. This is typical for the metal-induced gap states at insulator surfaces[56]. The valence band features (E= -4.0 ~ -1.5eV) are shifted to the shallower side (positive E) at the interface (C1 and C2). We noted that the energy of the s bands of the alkali metals becomes shallower in the order of Li < Na < K, corresponding to the electronegativity of these elements. It is then reasonable that the hybridized levels of the carbon and alkali metals become shallower in this order. Almost no DOS of the 4s electrons are found for K below E = -2eV, where the main valence states of diamond are located. It is consistent with the weak chemical interaction of K with diamond, and the stronger upward band bending at the K interface shown below.

The band bending can be estimated by DFT calculations without explicitly considering the dopants by watching

the shift in the valence states near the interface[57]. Without shallow dopant atoms, the length of the band bending region becomes infinitely long, and the bending energy can be obtained by comparing the LDOS features of the bulk semiconductor and that of the interface with the metal. The shift of the valence bands of diamond is evidenced in Fig. 9, in which the fourth layer carbon (C4) LDOS is plotted for (a) pure diamond(100) (vacuum interface), (b) Na/diamond(100), and (c) K/diamond(100) . In Fig.8(a), the LDOS is shifted to align the Fermi level, which should be located at the center of the band gap in the bulk. The upward shift (band bending) of the valence band of diamond at the Na interface is ~ 1.0eV and that of K is ~1.2 eV.

It is reported that the hydrogen termination of diamond reduces the negative charge of the NV centers (NV^0 increases while NV^- decreases)[30], while fluorine termination increases it [25,58]. This is explained by a band bending model in which the NV^- and NV^0 levels are located at 2.9eV[30,49] (or 2.0 eV[25,58]) and 1.2 eV[25,58] higher than the valence band maximum, respectively. When the surface band bending occurs to the shallower side (H-termination), the electronic level of the NV^- center becomes higher than the Fermi level and the negative charge is lost. The surface band bending occurs at the deeper side (F-termination), the NV^- center level becomes below the Fermi level and the negative charge is gained. In the present case, upward band bending occurs in the Na and K, and the threshold for losing an electron of NV^- is presumably passed only in the case of K, which produces a stronger band bending. If we assume that the NV^- level is 2.9eV[30,50] above the valence band maximum (VBM) and that the Fermi level is at half of the NV^- level and VBM, the threshold band bending for the charge of NV^- to escape is 1.45eV. This is close to the calculated band bending of 1.0 eV (Na) and 1.2eV (K), and the difference of 0.2eV between Na and K can affect the results at elevated temperatures.

Another point to mention is the probing depth of fluorescence (~1μm in the present case) and the depth of the band bending region. Although the band bending length can be estimated from the dopant concentration (~100nm in this case), it becomes greater if the co-dopants or defects can act as charge compensators. We speculate that the statistical deviation in the NV^- decrease by the K-treatment is related to the spatial distribution of the NV centers and other dopants.

Another important factor is the difference in the surface composition detected by XPS. The XPS results are

summarized as follows: (i) The chemical / electrical nature of the surface carbon atoms changes from pure diamond after the Na-annealing. (ii) The amount of the surface O-atoms becomes lower after the K-annealing (from 0.55 to 0.37 as O1s/C1s peak ratio), which suggests that the surface O-termination is partially replaced by H-termination. The latter is consistent with the report that H-termination reduces the NV^- ratio[25,29,30,35], and it may provide another explanation of the diminished NV^- fluorescent signal observed in the present experiment. Since the ethanol-water treatment to remove alkali metals after the annealing is a very complicated process, it is difficult to clarify its atomistic details. However, the clear difference between the Na and K-treatment effects in the XPS observation is surely related to the electronic interaction at the diamond-alkali metal interfaces revealed by the DFT calculations.

Finally, we compared our results with previous theoretical studies. Alkali metal (co-)absorption on a diamond surface with a monolayer thickness has been computationally studied [59,60]. It is noted that the Li monolayer adsorption gives the greatest negative electron affinity among the alkali metals. The difference between the monolayer adsorption and the bulk metal interface is mainly due to the existence of free electrons in the bulk metals.

5. Conclusions

We studied the interaction of diamond and Li, Na, and K liquids in an inert Ar atmosphere at high temperature. Significant etching by Li occurred at 600ºC or higher temperatures. Na induced a nm-thick surface roughness by heating at 800ºC for 24h. K did not induce any morphological change on the diamond surface. Photoluminescence measurements of the NV centers showed a decrease in the negatively charged NV^- compared to the neutral NV^0 only in the case of annealing with K. DFT calculations revealed upward band bending at the Na and K interfaces, and the bending is greater at the K interfaces. This result reasonably explains the behavior of the NV^- charge by annealing with K.

Acknowledgment

The photoluminescence measurement was done with the instrumental support of the Nanotechnology Platform at Hokkaido University offered by MEXT, Japan. The computational analysis was performed using supercomputers

at Hokkaido University and at ISSP, The University of Tokyo. Part of this research was financially supported by KAKENHI 17H03380.

References

[1] Z. Zhao, B. Xu, Y. Tian, Recent Advances in Superhard Materials, Annu. Rev. Mater. Res. 46 (2016) 383–406. https://doi.org/10.1146/annurev-matsci-070115-031649.

[2] L. Wei, P.K. Kuo, R.L. Thomas, T.R. Anthony, W.F. Banholzer, Thermal conductivity of isotopically modified single crystal diamond, Phys. Rev. Lett. 70 (1993) 3764–3767. https://doi.org/10.1103/PhysRevLett.70.3764.

[3] H. Kawarada, Hydrogen-terminated diamond surfaces and interfaces, Surf. Sci. Rep. 26 (1996) 205–259. https://doi.org/10.1016/s0167-5729(97)80002-7.

[4] I. Aharonovich, A.D. Greentree, S. Prawer, Diamond photonics, Nat. Photonics. 5 (2011) 397–405. https://doi.org/10.1038/nphoton.2011.54.

[5] A. Nieto, J. Kim, O. V. Penkov, D.E. Kim, J.M. Schoenung, Elevated temperature wear behavior of thermally sprayed WC-Co/nanodiamond composite coatings, Surf. Coatings Technol. 315 (2017) 283–293. https://doi.org/10.1016/j.surfcoat.2017.02.048.

[6] I. Bello, Y.M. Chong, Q. Ye, Y. Yang, B. He, O. Kutsay, H.E. Wang, C. Yan, S.K. Jha, J.A. Zapien, W.J. Zhang, Materials with extreme properties: Their structuring and applications, Vacuum. 86 (2012) 575–585. https://doi.org/10.1016/j.vacuum.2011.08.010.

[7] D.T. Morelli, J.P. Heremans, G.A. Slack, Estimation of the isotope effect on the lattice thermal conductivity of group IV and group III-V semiconductors, Phys. Rev. B - Condens. Matter Mater. Phys. 66 (2002) 195304. https://doi.org/10.1103/PhysRevB.66.195304.

[8] S. Ma, N. Zhao, C. Shi, E. Liu, C. He, F. He, L. Ma, Mo_2C coating on diamond: Different effects on thermal conductivity of diamond/Al and diamond/Cu composites, Appl. Surf. Sci. 402 (2017) 372–383. https://doi.org/10.1016/j.apsusc.2017.01.078.

[9] Z. Cheng, L. Yates, J. Shi, M.J. Tadjer, K.D. Hobart, S. Graham, Thermal conductance across β-Ga_2O_3-diamond van der Waals heterogeneous interfaces, APL Mater. 7 (2019) 031118. https://doi.org/10.1063/1.5089559.

[10] K. Yoshida, H. Morigami, Thermal properties of diamond/copper composite material, Microelectron. Reliab. 44 (2004) 303–308. https://doi.org/10.1016/S0026-2714(03)00215-4.

[11] S. V. Kidalov, F.M. Shakhov, Thermal conductivity of diamond composites, Materials (Basel). 2 (2009) 2467–2495. https://doi.org/10.3390/ma2042467.

[12] V.D. Blank, V.S. Bormashov, S.A. Tarelkin, S.G. Buga, M.S. Kuznetsov, D. V. Teteruk, N. V. Kornilov, S.A. Terentiev, A.P. Volkov, Power high-voltage and fast response Schottky barrier diamond diodes, Diam. Relat. Mater. 57 (2015) 32–36. https://doi.org/10.1016/j.diamond.2015.01.005.

[13] A. Hiraiwa, H. Kawarada, Figure of merit of diamond power devices based on accurately estimated impact ionization processes, J. Appl. Phys. 114 (2013) 34506. https://doi.org/10.1063/1.4816312.

[14] A. Denisenko, E. Kohn, Diamond power devices. Concepts and limits, Diam. Relat. Mater. 14 (2005) 491–498. https://doi.org/10.1016/j.diamond.2004.12.043.

[15] S. Shikata, Single crystal diamond wafers for high power electronics, Diam. Relat. Mater. 65 (2016) 168–175. https://doi.org/10.1016/j.diamond.2016.03.013.

[16] J.L. Hudgins, G.S. Simin, E. Santi, M.A. Khan, An assessment of wide bandgap semiconductors for power devices, IEEE Trans. Power Electron. 18 (2003) 907–914. https://doi.org/10.1109/TPEL.2003.810840.

[17] S. Yamasaki, E. Gheeraert, Y. Koide, Doping and interface of homoepitaxial diamond for electronic applications, MRS Bull. 39 (2014) 499–503. https://doi.org/10.1557/mrs.2014.100.

[18] A. Sawant, D. Kwak, I. Lee, M. Chung, E.M. Choi, Stand-off radiation detection techniques, Rev. Sci. Instrum. 91 (2020) 071501. https://doi.org/10.1063/1.5134088.

[19] M. Werner, R. Locher, Growth and application of undoped and doped diamond films, Reports Prog. Phys. 61 (1998) 1665–1710. https://doi.org/10.1088/0034-4885/61/12/002.

[20] G.J. Schmid, J.A. Koch, R.A. Lerche, M.J. Moran, A neutron sensor based on single crystal CVD diamond, Nucl. INSTRUMENTS METHODS Phys. Res. Sect. A-ACCELERATORS SPECTROMETERS Detect. Assoc. Equip. 527 (2004) 554–561. https://doi.org/10.1016/j.nima.2004.03.199.

[21] G. Balasubramanian, P. Neumann, D. Twitchen, M. Markham, R. Kolesov, N. Mizuochi, J. Isoya, J. Achard, J. Beck, J. Tissler, V. Jacques, P.R. Hemmer, F. Jelezko, J. Wrachtrup, Ultralong spin coherence time in isotopically engineered diamond, Nat Mater. 8 (2009) 383–387. https://doi.org/10.1038/nmat2420.

[22] J. Tisler, G. Balasubramanian, B. Naydenov, R. Kolesov, B. Grotz, R. Reuter, J.P. Boudou, P.A. Curmi, M. Sennour, A. Thorel, M. Borsch, K. Aulenbacher, R. Erdmann, P.R. Hemmer, F. Jelezko, J. Wrachtrup, Fluorescence and spin properties of defects in single digit nanodiamonds, ACS Nano. 3 (2009) 1959–1965. https://doi.org/10.1021/nn9003617.

[23] F. Hilser, G. Burkard, All-optical control of the spin state in the NV- center in diamond, Phys. Rev. B. 86 (2012) 125204. https://doi.org/10.1103/PhysRevB.86.125204.

[24] M.S. Grinolds, M. Warner, K. De Greve, Y. Dovzhenko, L. Thiel, R.L. Walsworth, S. Hong, P. Maletinsky, A. Yacoby, Subnanometre resolution in three-dimensional magnetic resonance imaging of individual dark spins, Nat Nanotechnol. 9 (2014) 279–284. https://doi.org/10.1038/nnano.2014.30.

[25] V. Petráková, A. Taylor, I. Kratochvílová, F. Fendrych, J. Vacík, J. Kučka, J. Štursa, P. Cígler, M. Ledvina, A. Fišerová, P. Kneppo, M. Nesládek, Luminescence of nanodiamond driven by atomic functionalization: Towards novel detection principles, Adv. Funct. Mater. 22 (2012) 812–819. https://doi.org/10.1002/adfm.201101936.

[26] J. Forneris, S. Ditalia Tchernij, A. Tengattini, E. Enrico, V. Grilj, N. Skukan, G. Amato, L. Boarino, M. Jakšić, P. Olivero, Electrical control of deep NV centers in diamond by means of sub-superficial graphitic micro-electrodes, Carbon N. Y. 113 (2017) 76–86. https://doi.org/10.1016/j.carbon.2016.11.031.

[27] B. Grotz, M. V. Hauf, M. Dankerl, B. Naydenov, S. Pezzagna, J. Meijer, F. Jelezko, J. Wrachtrup, M. Stutzmann, F. Reinhard, J.A. Garrido, Charge state manipulation of qubits in diamond, Nat. Commun. 3 (2012). https://doi.org/10.1038/ncomms1729.

[28] Y. Doi, T. Fukui, H. Kato, T. Makino, S. Yamasaki, T. Tashima, H. Morishita, S. Miwa, F. Jelezko, Y. Suzuki, N. Mizuochi, Pure negatively charged state of the NV center in n -type diamond, Phys. Rev. B. 93 (2016) 081203. https://doi.org/10.1103/PhysRevB.93.081203.

[29] L. Rondin, G. Dantelle, A. Slablab, F. Grosshans, F. Treussart, P. Bergonzo, S. Perruchas, T. Gacoin, M. Chaigneau, H.C. Chang, V. Jacques, J.F. Roch, Surface-induced charge state conversion of nitrogen-vacancy defects in nanodiamonds, Phys. Rev. B. 82 (2010) 115449. https://doi.org/10.1103/PhysRevB.82.115449.

[30] M. V. Hauf, B. Grotz, B. Naydenov, M. Dankerl, S. Pezzagna, J. Meijer, F. Jelezko, J. Wrachtrup, M. Stutzmann,

F. Reinhard, J.A. Garrido, Chemical control of the charge state of nitrogen-vacancy centers in diamond, Phys. Rev. B - Condens. Matter Mater. Phys. 83 (2011) 081304. https://doi.org/10.1103/PhysRevB.83.081304.

[31] D. Bluvstein, Z. Zhang, A.C.B. Jayich, Identifying and Mitigating Charge Instabilities in Shallow Diamond Nitrogen-Vacancy Centers, Phys. Rev. Lett. 122 (2019) 076101. https://doi.org/10.1103/PhysRevLett.122.076101.

[32] Y. Doi, T. Makino, H. Kato, D. Takeuchi, M. Ogura, H. Okushi, H. Morishita, T. Tashima, S. Miwa, S. Yamasaki, P. Neumann, J. Wrachtrup, Y. Suzuki, N. Mizuochi, Deterministic electrical charge-state initialization of single nitrogen-vacancy center in diamond, Phys. Rev. X. 4 (2014) 011057. https://doi.org/10.1103/PhysRevX.4.011057.

[33] S. Karaveli, O. Gaathon, A. Wolcott, R. Sakakibara, O.A. Shemesh, D.S. Peterka, E.S. Boyden, J.S. Owen, R. Yuste, D. Englund, Modulation of nitrogen vacancy charge state and fluorescence in nanodiamonds using electrochemical potential, Proc. Natl. Acad. Sci. U. S. A. 113 (2016) 3938–3943. https://doi.org/10.1073/pnas.1504451113.

[34] C. Schreyvogel, V. Polyakov, R. Wunderlich, J. Meijer, C.E. Nebel, Active charge state control of single NV centres in diamond by in-plane Al-Schottky junctions, Sci. Rep. 5 (2015) 12160. https://doi.org/10.1038/srep12160.

[35] H. Yamano, S. Kawai, K. Kato, T. Kageura, M. Inaba, T. Okada, I. Higashimata, M. Haruyama, T. Tanii, K. Yamada, S. Onoda, W. Kada, O. Hanaizumi, T. Teraji, J. Isoya, H. Kawarada, Charge state stabilization of shallow nitrogen vacancy centers in diamond by oxygen surface modification., Jpn. J. Appl. Phus. 56 (2017) 04CK08. https://doi.org/10.7657/JJAP.56.04CK08.

[36] K. Nakanishi, H. Kuroshima, T. Matsumoto, T. Inokuma, N. Tokuda, Atomically flat diamond (100) surface formation by anisotropic etching of solid-solution reaction of carbon into nickel, Diam. Relat. Mater. 68 (2016) 127–130. https://doi.org/10.1016/j.diamond.2016.06.011.

[37] M. Nagai, Y. Nakamura, T. Yamada, T. Tabakoya, T. Matsumoto, T. Inokuma, C.E. Nebel, T. Makino, S. Yamasaki, N. Tokuda, Formation of U-shaped diamond trenches with vertical {111} sidewalls by anisotropic etching of diamond (110) surfaces, Diam. Relat. Mater. 103 (2020) 107713. https://doi.org/10.1016/j.diamond.2020.107713.

[38] M. Nagai, K. Nakanishi, H. Takahashi, H. Kato, T. Makino, S. Yamasaki, T. Matsumoto, T. Inokuma, N. Tokuda, Anisotropic diamond etching through thermochemical reaction between Ni and diamond in high-Temperature water vapour, Sci. Rep. 8 (2018) 6687. https://doi.org/10.1038/s41598-018-25193-2.

[39] W. Smirnov, J.J. Hees, D. Brink, W. Müller-Sebert, A. Kriele, O.A. Williams, C.E. Nebel, Anisotropic etching of diamond by molten Ni particles, Appl. Phys. Lett. 97 (2010) 2008–2011. https://doi.org/10.1063/1.3480602.

[40] T. Schuelke, T.A. Grotjohn, Diamond polishing, Diam. Relat. Mater. 32 (2013) 17–26. https://doi.org/10.1016/j.diamond.2012.11.007.

[41] X.B. Cheng, M.Q. Zhao, C. Chen, A. Pentecost, K. Maleski, T. Mathis, X.Q. Zhang, Q. Zhang, J. Jiang, Y. Gogotsi, Nanodiamonds suppress the growth of lithium dendrites, Nat. Commun. 8 (2017) 1–9. https://doi.org/10.1038/s41467-017-00519-2.

[42] Y. Liu, Y.K. Tzeng, D. Lin, A. Pei, H. Lu, N.A. Melosh, Z.X. Shen, S. Chu, Y. Cui, An Ultrastrong Double-Layer Nanodiamond Interface for Stable Lithium Metal Anodes, Joule. 2 (2018) 1595–1609. https://doi.org/10.1016/j.joule.2018.05.007.

[43] G. Kresse, J. Hafner, Ab initio molecular dynamics for liquid metals, Phys. Rev. B. 47 (1993) 558–561. https://doi.org/10.1103/PhysRevB.47.558.

[44] V.N. Mochalin, O. Shenderova, D. Ho, Y. Gogotsi, The properties and applications of nanodiamonds, Nat Nanotechnol. 7 (2012) 11–23. https://doi.org/10.1038/nnano.2011.209.

[45] M. Hulman, H. Kuzmany, O. Dubay, G. Kresse, L. Li, Z.K. Tang, P. Knoll, R. Kaindl, Raman spectroscopy of single wall carbon nanotubes grown in zeolite crystals, Carbon N. Y. 42 (2004) 1071–1075. https://doi.org/10.1016/j.carbon.2003.12.039.

[46] D. Joubert, From ultrasoft pseudopotentials to the projector augmented-wave method, Phys. Rev. B - Condens. Matter Mater. Phys. 59 (1999) 1758–1775. https://doi.org/10.1103/PhysRevB.59.1758.

[47] A. Jain, S.P. Ong, G. Hautier, W. Chen, W.D. Richards, S. Dacek, S. Cholia, D. Gunter, D. Skinner, G. Ceder, K. a. Persson, The Materials Project: A materials genome approach to accelerating materials innovation, APL Mater. 1 (2013) 11002. https://doi.org/10.1063/1.4812323.

[48] Y. Yao, Y. Ishikawa, Y. Sugawara, H. Yamada, A. Chayahara, Y. Mokuno, Fast removal of surface damage layer from single crystal diamond by using chemical etching in molten KCl + KOH solution, Diam. Relat. Mater. 63 (2016) 86–90. https://doi.org/10.1016/j.diamond.2015.10.003.

[49] S. Jin, J.E. Graebner, M. McCormack, T.H. Tiefel, A. Katz, W.C. Dautremont-Smith, Shaping of diamond films by etching with molten rare-earth metals, Nature. 362 (1993) 822–824. https://doi.org/10.1038/362822a0.

[50] A. Bhaumik, R. Sachan, J. Narayan, Tunable charge states of nitrogen-vacancy centers in diamond for ultrafast quantum devices, Carbon N. Y. 142 (2019) 662–672. https://doi.org/10.1016/j.carbon.2018.10.084.

[51] S. D. Tchernij, T. Lühmann, E. Corte, F. Sardi, F. Picollo, P. Traina, M. Brajković, A. Crnjac, S. Pezzagna, Ž. Pastuović, I. P. Degiovanni, E. Moreva, P. Aprà, P. Olivero, Z. Siketić, J. Meijer, M. Genovese, J. Forneris, Fluorine-based color centers in diamond, Scientific Reports 10 (2020) 21537. https://doi.org/10.1038/s41598-020-78436-6

[52] A. Fujimoto, Y. Yamada, M. Koinuma, S. Sato, Origins of sp3 C peaks in C1s X-ray photoelectron spectra of carbon materials, Analytical Chemistry 88 (2016) 6110-6114. https://doi.org/10.1021/acs.analchem.6b01327.

[53] Y. Kawabata, J. Taniguchi, I. Miyamoto, XPS studies on damage evaluation of single-crystal diamond chips processed with ion beam etching and reactive ion beam assisted chemical etching, Diamond and Related Materials 13 (2004) 93-98. https://doi.org/10.1016/j.diamond.2003.09.005

[54] S. Filippov, J. Klarbring, U. Haüssermann, S.I. Simak, Temperature-induced phase transition and Li self-diffusion in Li_2C_2: A first-principles study, Phys. Rev. Mater. 3 (2019) 023602. https://doi.org/10.1103/PhysRevMaterials.3.023602.

[55] J. Robertson, Diamond Like amorphous carbon, Mater. Sci. Eng. R. 37 (2002) 129–281.

[56] G. Bordier, C. Noguera, Electronic structure of a metal-insulator interface: Towards a theory of nonreactive adhesion, Phys. Rev. B. 44 (1991) 6361.

[57] Y. Jiao, A. Hellman, Y. Fang, S. Gao, M. Käll, Schottky barrier formation and band bending revealed by first-principles calculations, Sci. Rep. 5 (2015) 11374. https://doi.org/10.1038/srep11374.

[58] T.W. Shanley, A.A. Martin, I. Aharonovich, M. Toth, Localized chemical switching of the charge state of nitrogen-vacancy luminescence centers in diamond, Appl. Phys. Lett. 105 (2014) 063103. https://doi.org/10.1063/1.4883229.

[59] K.M. O'Donnell, T.L. Martin, M.T. Edmonds, A. Tadich, L. Thomsen, J. Ristein, C.I. Pakes, N.A. Fox, L. Ley, Photoelectron emission from lithiated diamond, Phys. Status Solidi Appl. Mater. Sci. 211 (2014) 2209–2222. https://doi.org/10.1002/pssa.201431414.

[60] K.M. O'donnell, T.L. Martin, N.L. Allan, Light Metals on Oxygen-Terminated Diamond (100): Structure and Electronic Properties, Chem. Mater. 27 (2015) 1306–1315. https://doi.org/10.1021/cm5043155.

Figure captions

Fig.1: Sample preparation. (a) A picture and description of the reaction vessel. (b) Crystalline diamond particles.

Fig.2: Laser microscope image of diamond grains before (a,c,e) and after (b,d,f) the molten alkali metal treatment. b: Li, 650ºC, 20min.; d: Na, 800ºC, 24h; f: K, 800ºC, 24h. a and b, c and d, and e and f show the same particles, respectively.

Fig.3: Surface morphology analysis of diamond surface etched by Li melt treatment. Left panel: A laser microscope image. Right panel: Cross section plots along A-B and C-D lines in the image.

Fig. 4: Optical microscope images of before and after the annealing with lithium for 20 min. At 600ºC, flat region (a) only showed etching from the edges and from dimples. Regions with imperfections (b) showed substantial etching. At 625ºC, etching of the flat region started to occur(c). Regions with imperfections (d) showed more etching.

Fig.5: Photoluminescence before and after the heat treatment in a vacuum(a), with Li(b), Na(c) and K(d). Insets show the NV^- peaks after subtracting the broad background due to phonon-involved fluorescence and normalization by the peak around 573 nm (diamond Raman and NV^0).

Fig.6: XPS (a)C1s and (b)O1s of the diamond crystalline particles without treatment and after annealing with Na and K at 800ºC for 24h.

Fig.7: Optimized structures of alkali metal / diamond interfaces by DFT calculations.

Fig.8: Atomic-layer decomposed local density of states (LDOS) of alkali metal / diamond interfaces. Labels for the atoms are shown in Fig. 7.

Fig.9: Valence band LDOS at the 4th layer carbon (C4). (a) Interface with vacuum (used as reference of pristine diamond), (b) Interface with Na, (c) Interface with K. (a) is shifted to align the Fermi level with those of (b) and (c).

Fig.1

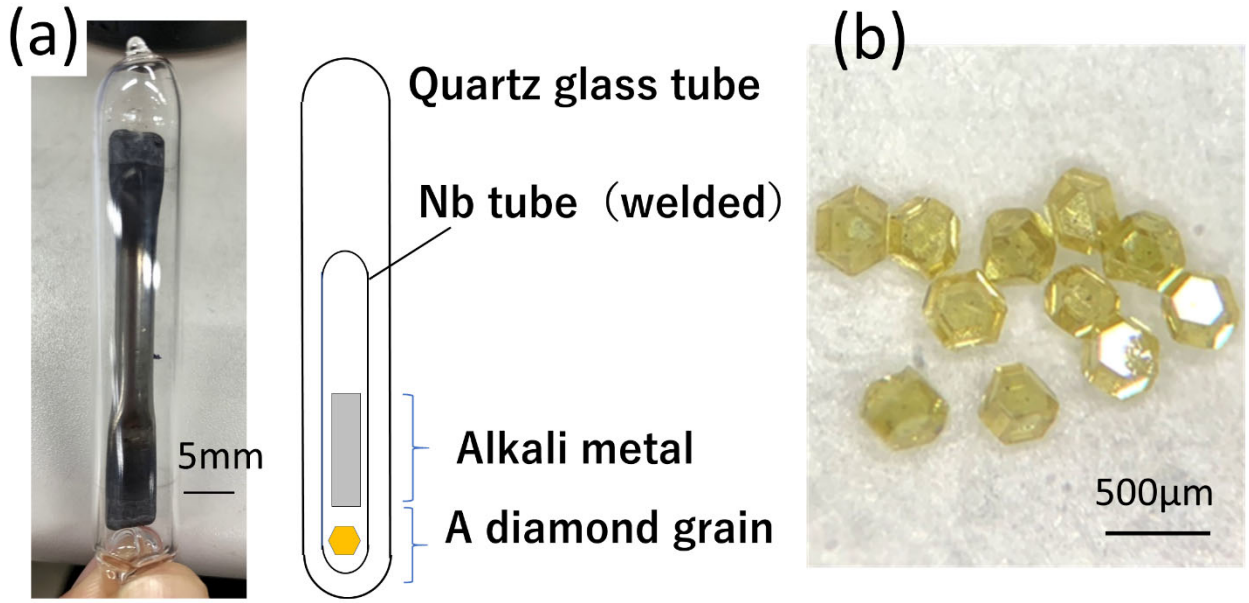
(a)
5mm
Quartz glass tube
Nb tube（welded）
Alkali metal
A diamond grain
(b)
500μm

Fig.2

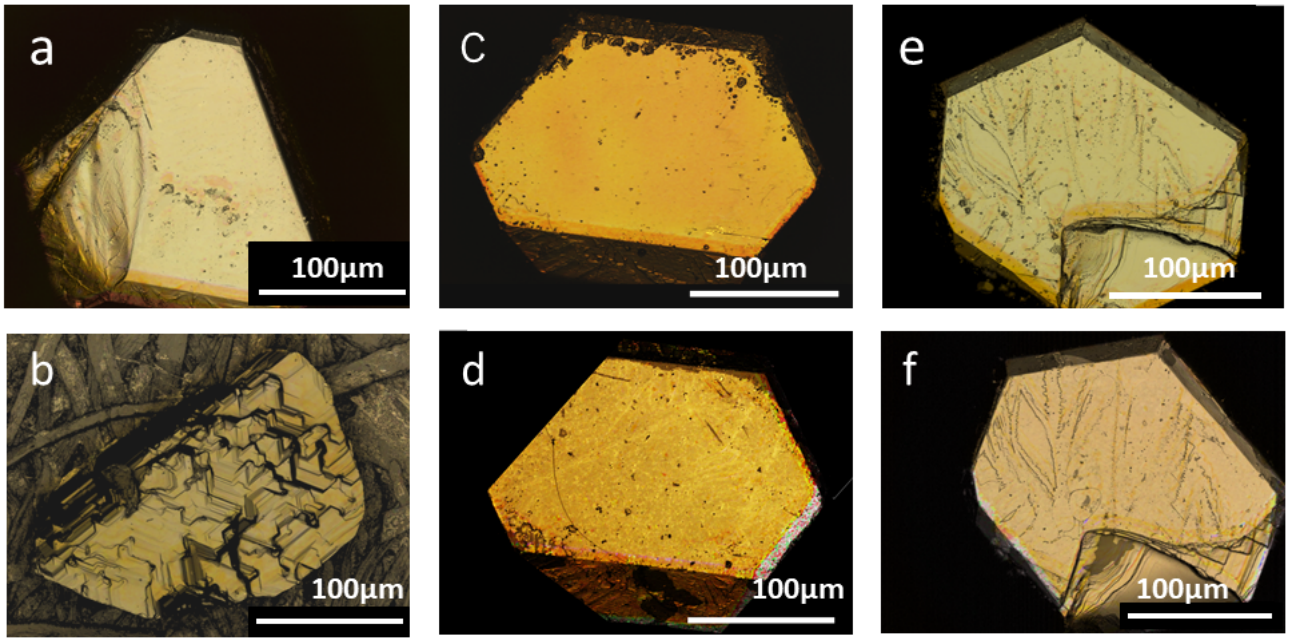
a
100μm
c
100μm
e
100μm
b
100μm
d
100μm
f
100μm

Fig.3

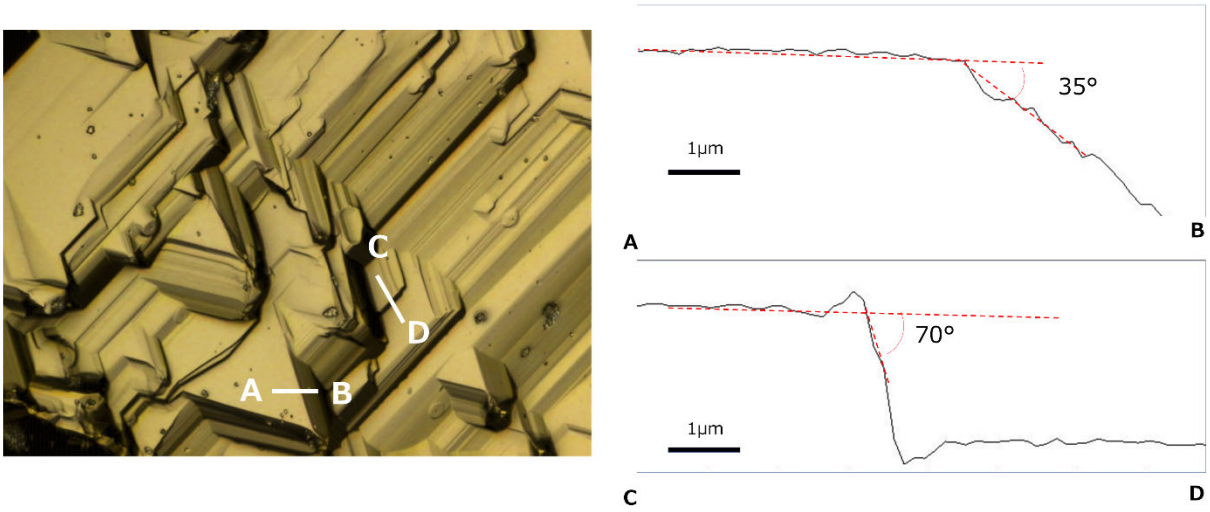

Fig.4

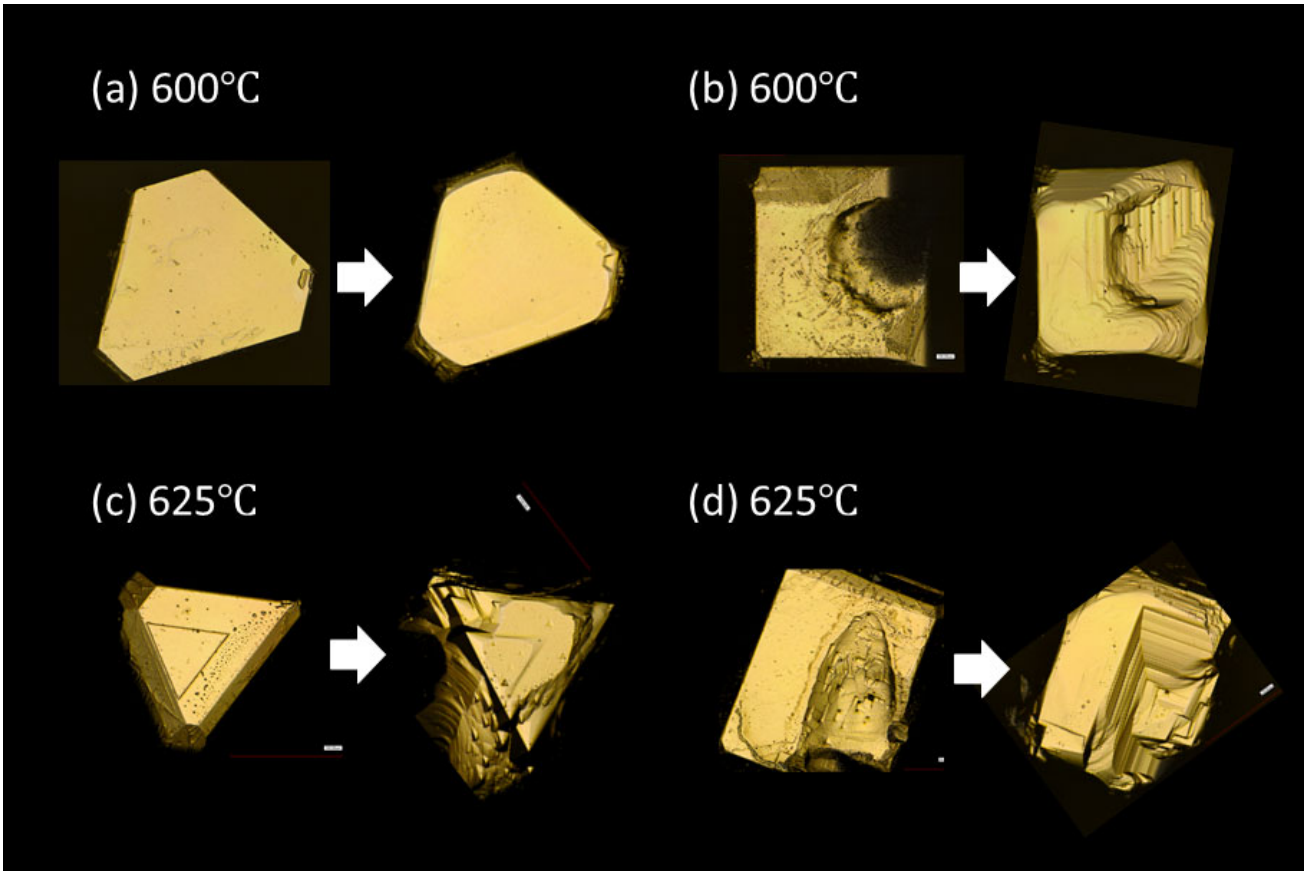

Fig.5

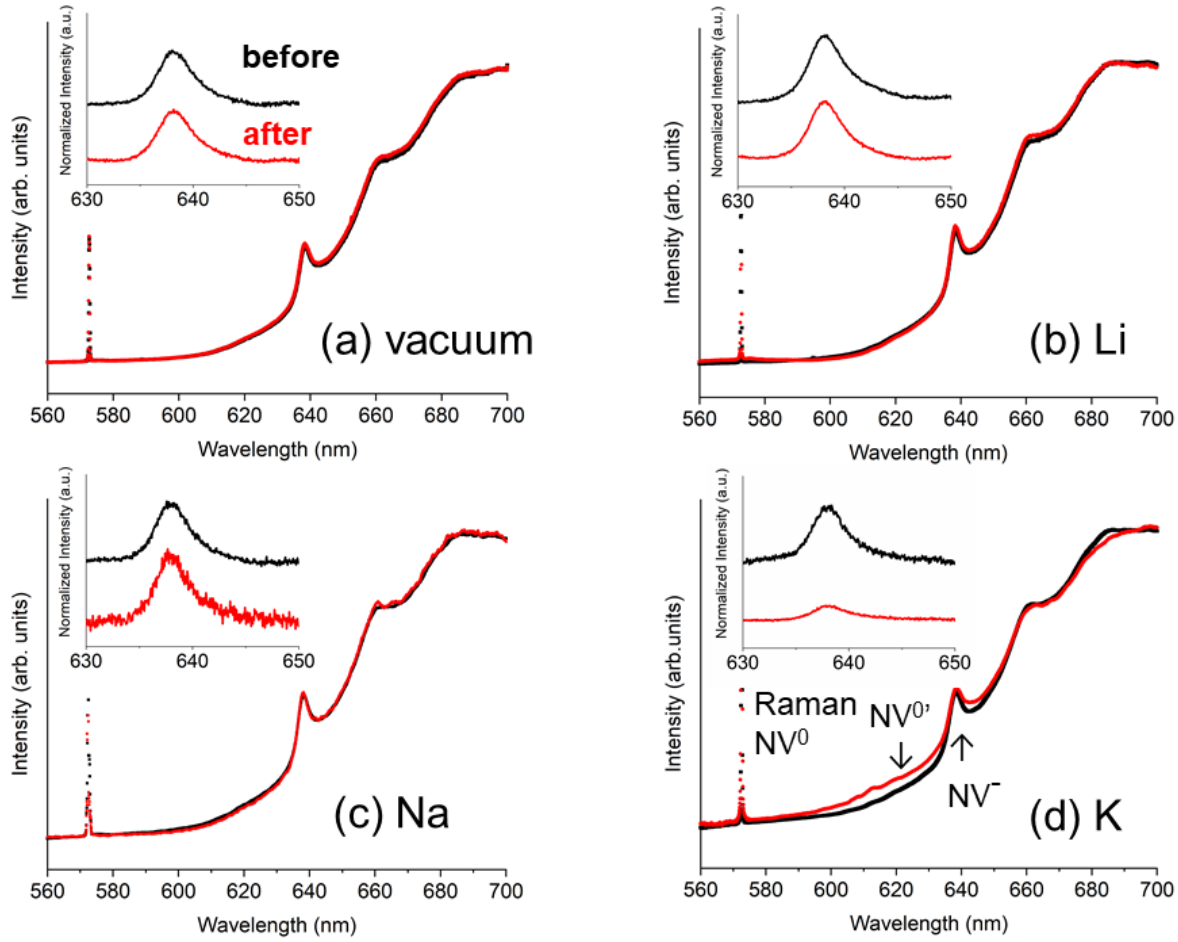
before
after
Normalized Intensity (a.u.)
630
640
650
Intensity (arb. units)
(a) vacuum
560
580
600
620
640
660
680
700
Wavelength (nm)
(b) Li
(c) Na
Raman
NV0
NV0,
NV-
(d) K

Fig.6

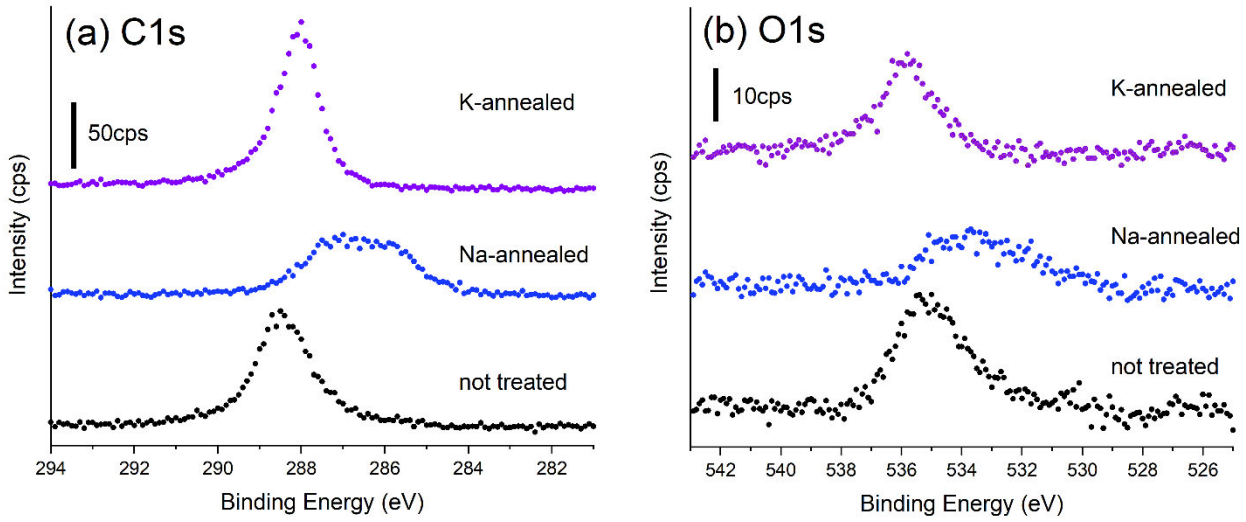
(a) C1s
50cps
K-annealed
Na-annealed
not treated
Intensity (cps)
294
292
290
288
286
284
282
Binding Energy (eV)
(b) O1s
10cps
K-annealed
Na-annealed
not treated
Intensity (cps)
542
540
538
536
534
532
530
528
526
Binding Energy (eV)

Fig.7

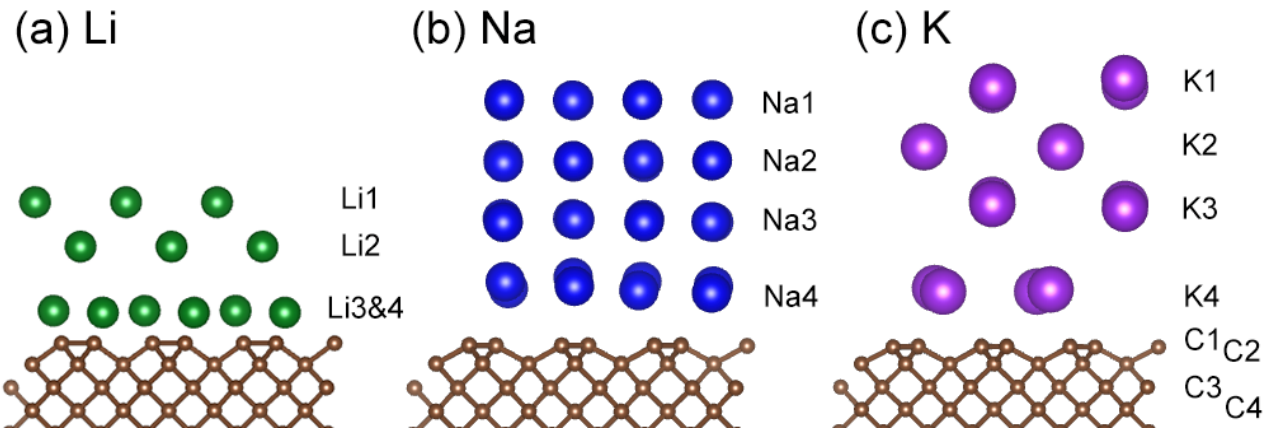
(a) Li
Li1
Li2
Li3&4
(b) Na
Na1
Na2
Na3
Na4
(c) K
K1
K2
K3
K4
C1
C2
C3
C4

Fig.8

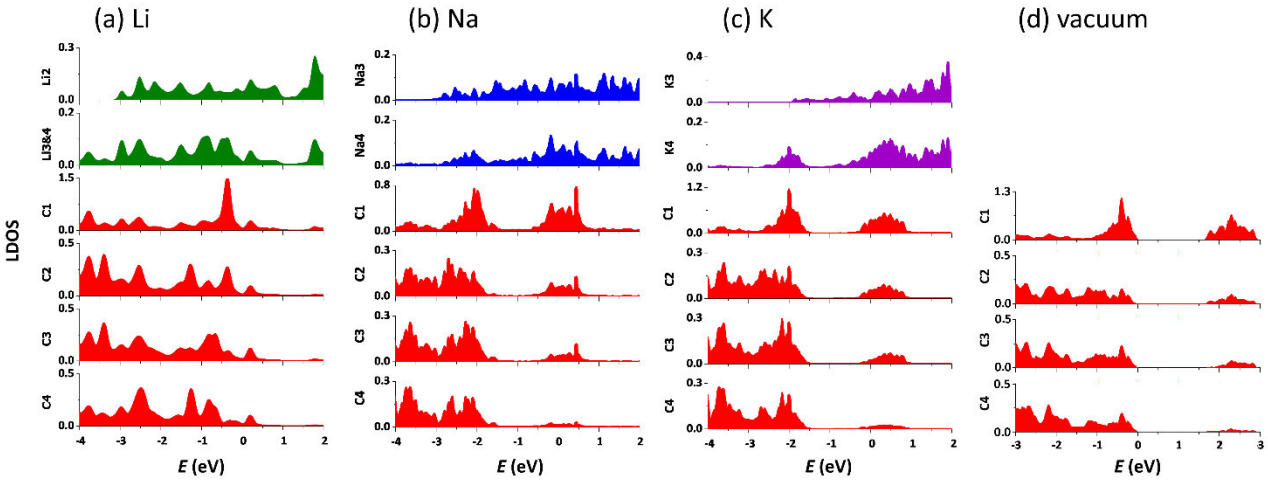
(a) Li
(b) Na
(c) K
(d) vacuum
LDOS
Li2
LI384
Na3
Na4
K3
K4
C1
C2
C3
C4
E (eV)

Fig.9

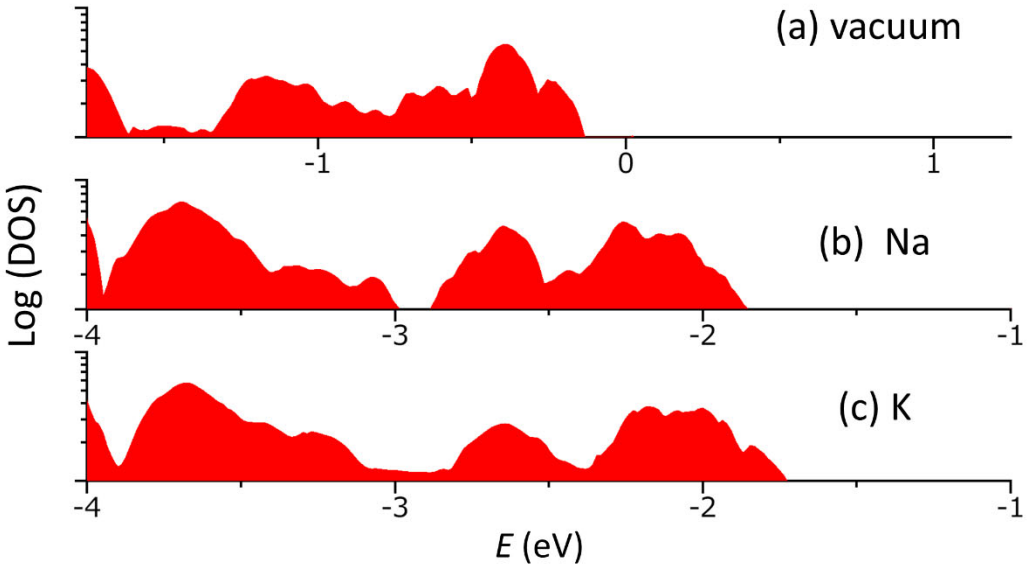
(a) vacuum
(b) Na
(c) K
Log (DOS)
E (eV)